

Origin of ellipticity of high-order harmonics generated by a two-color laser field in the cross-polarized configuration

S. Stremoukhov,^{1,2,*} A. Andreev,¹ B. Vodungbo,^{3,4} P. Salières,⁵ B. Mahieu,³ and G. Lambert³

¹*Faculty of Physics, Lomonosov Moscow State University, Leninskie Gory, 1, building 2, Moscow 119991, Russia*

²*National Research Centre “Kurchatov Institute,” 1 Akademika Kurchatova Place, Moscow 123182, Russia*

³*LOA, ENSTA ParisTech, CNRS, Ecole polytechnique, Université Paris-Saclay, 828 Boulevard des Maréchaux, 91762 Palaiseau cedex, France*

⁴*Sorbonne Universités, UPMC Université Paris 06, UMR 7614, LCPMR, 75005 Paris, France*

and CNRS, UMR 7614, LCPMR, 75005 Paris, France

⁵*CEA-Saclay, IRAMIS/LIDyL, 91191 Gif-sur-Yvette, France*

(Received 18 December 2015; published 29 July 2016)

Recently several techniques demonstrated the production of elliptically polarized high harmonics. One of these techniques consists of the interaction in a noble gas of two-color laser beams having orthogonal linear polarizations. Here we present the theoretical explanation of such a result observed in Lambert *et al.* [*Nat. Commun.* **6**, 6167 (2015)]. Numerical calculations based on the nonperturbative light-atom interaction theory reproduce well the experimental data. The degree of polarization is analyzed for different harmonic orders and found to be high. With the help of a simplified theoretical model it is shown that the degree of harmonic ellipticity depends mainly on the population of atomic state sublevels with different angular momentum projections.

DOI: [10.1103/PhysRevA.94.013855](https://doi.org/10.1103/PhysRevA.94.013855)

I. INTRODUCTION

High-order harmonic generation (HHG) in gases is a well-known technique leading to the generation of coherent ultraviolet to soft x-ray femtosecond pulses [1]. To overcome its major limitation for applications, i.e., the weak number of photons, a lot of methods have been developed, using different media (gases [2], molecules [3], plasma plumes [4], and mixtures of gases [5,6]) different optical geometries [7–9], and different laser sources (single-color [10], two-color [11], three-color [12], even five-color setups [13]). Another fundamental limitation was, up to recent results, the restriction to linear polarizations which prevents for instance the development of a number of polarization spectroscopy methods, especially based on dichroism. Indeed, the polarization of the harmonics coincides with the polarization of the driving laser field. When harmonics are produced by an elliptically polarized laser field, they have nonzero ellipticity [14–16] but a weak number of photons since the efficiency of the generating process drops dramatically along with the degree of ellipticity [17,18]. In order to solve this issue, several techniques have been proposed [19–30], but only a few of them have produced elliptically polarized high harmonics with non-negligible efficiency. The first method is based on the use of prealigned molecules [31,32]. This approach requires, however, a complex optical setup, and the measured ellipticity does not exceed 35% and only in the narrow part of the generated spectrum. Alternatively, the linear polarization of harmonics can be converted into circular polarization using a reflector phase shifter [33]. This system, technically challenging, reduces additionally the harmonic signal by one to two orders of magnitude depending on the degree of circular polarization required and is limited to photon energies up to about 70 eV. Recently, three methods for producing intense and highly elliptical harmonics have been demonstrated almost simultaneously [34–36]. The first scheme, presented previously in

Ref. [37], is based on the use of two-color counter-rotating elliptically polarized beams [34]. In this setup, both beams are separated into two arms and recombined spatially and temporally inside the gas medium, constituting a quite complex setup. Yet, the advantages of this scheme are numerous: The polarization of the generated harmonics is completely controlled, circularly polarized harmonics can be generated, and investigation of the behavior of spin angular momentum in the HHG process is enabled [38,39]. In the second scheme, the use of the below-threshold atomic resonances and continuum resonances allows to produce efficient low-order quasicircular harmonics in an elliptically polarized single-color laser field [35]. The apparent ellipticity achieved in that experiment is quite high (up to 75%), although it is only an upper bound for the ellipticity, not ruling out the presence of randomly polarized radiation [35]. Also, such a high value of ellipticity is only available at the resonance energies for gases with complex structures. Third, the scheme in which is here focused is presented in Ref. [36] and is based on a two-color laser field in the cross-polarized configuration. It simply consists of a linearly polarized fundamental radiation (ω) which generates its second harmonic (2ω) by means of a β -barium borate (BBO) crystal placed in the laser path. The polarization of the second harmonic is also linear but orthogonal to the one of the fundamental. As for the first scheme, a proof that the generated radiation is polarized at least partially is brought by the study of a typical polarization-sensitive phenomenon, such as the x-ray magnetic circular dichroism.

Here is presented a detailed theoretical description of the phenomena observed in Ref. [36], which helps to discover the origin of the high elliptical harmonics in the case of the orthogonally polarized waves. The theory describes the break in the temporal symmetry appearing in the process of an atom interacting with a two-color laser field and even predicts the appearance of both even and odd high-order harmonics with a high degree of ellipticity.

According to traditional studies, due to the temporal symmetry: (1) the harmonics generated in a $\omega + 2\omega$ field

*Corresponding author: sustrem@gmail.com

with components linearly and orthogonally polarized and both with relatively weak intensity should be linearly polarized, and (2) the polarization direction of odd harmonics should coincide with the polarization direction of ω , and the polarization direction of even harmonics should coincide with the polarization direction of 2ω [40]. This conclusion follows from the perturbation theory analysis and was obtained for the p -ground-state atom under strong assumptions: (i) only the $m = 0$ (m —projection of the orbital quantum number) sublevel of the ground state was taken into account as for other sublevels of both ground and continuum states—as a consequence the impact of all the other projections of the orbital quantum number were neglected; (ii) the impact of excited bound states on the HHG process was not taken into account, and the whole analysis is valid when the ground state is not preexcited. Otherwise saying the analysis presented in Ref. [40] can be applied to a medium consisting of atoms interacting with a sufficiently weak laser field. Indeed, a s state has the orbital quantum number $l = 0$ and its projection $m = 0$. The states with the other symmetries (p , d , f , etc.) have more than one m . As short femtosecond laser pulses are here considered and such pulses have broad energy spectra, different m 's should be taken into account because the wave functions corresponding to different m 's will make different impacts on the atomic current as well as on the high harmonic spectrum. In the experiments [36] considered here, neon (Ne) atomic gas has been used. With the ground state of Ne being a $2p$ state, the impact of the different m 's in the atomic current has been analyzed analytically. The result of this analysis, which is valid to describe the atomic response to a weak field [40], clearly provides the origin of the observed ellipticity. To describe the features of the HHG at a moderate intensity (which is used in the experiment [36]) one should use a more advanced model of the atomic energy structure where both discrete and continuum states are accounted. The results of these numerical simulations, presented further in the paper, are in excellent agreement with the results of experimental measurements, which opens a way to the interpretation of the rare gas interaction with multicomponent laser fields. The degree of polarization of the generated radiation is also discussed in the coming sections.

The paper is organized as follows. In Sec. II a short summary of the theoretical approach is presented, and the numerical model which has been used in the numerical simulations is discussed. In addition, the results of two tests showing the good validity of the model for describing the experimentally observed phenomena are provided. Section III is devoted to the description of the experimental environment and to the comparison between the experimental and the simulated data. The degree of polarization of the generated harmonics is evaluated in Sec. IV. In Sec. V, we provide further insight into the origin of this high ellipticity. The conclusions are presented in Sec. VI.

II. THEORY AND NUMERICAL MODEL

This section provides a short summary of the basic principles of nonperturbative theory and specific details of the numerical model used here. The detailed description of the theory is given in Ref. [41].

The Schrödinger equation for an atom interacting with an external electromagnetic field is as follows:

$$i\hbar \frac{\partial \psi(\vec{r}, t)}{\partial t} = \left[\frac{1}{2m} \left(\vec{p} - \frac{q}{c} \vec{A}(t) \right)^2 + U(r) \right] \psi(\vec{r}, t). \quad (1)$$

To solve Eq. (1) a nontraditional basis of functions $\varphi_N(\vec{r}, t)$ is used which is the exact solution of the boundary value problem for an atom in the external field,

$$\left[\frac{1}{2m} \left(\vec{p} - \frac{q}{c} \vec{A}(t) \right)^2 + U(r) \right] \varphi_N(\vec{r}, t) = E_N \varphi_N(\vec{r}, t). \quad (2)$$

The operator of the boundary value problem (2) coincides with the Hamiltonian of Eq. (1), so, these two equations have the same symmetry properties. The eigenfunctions $\varphi_N(\vec{r}, t)$ can be analytically expressed in terms of eigenfunctions $u_n(\vec{r})$ for the free-atom boundary value problem,

$$\varphi_N(\vec{r}, t) = \hat{V}^{-1} u_n(\vec{r}), \quad \hat{V} = \exp \left(-i \frac{q}{\hbar c} \vec{A}(t) \vec{r} \right).$$

Similar to the set of free-atom eigenfunctions $u_n(\vec{r})$ which form a complete basis of the orthonormal functions, the eigenfunctions $\varphi_N(\vec{r}, t)$ of the boundary value problem (2) for “an atom in the external field” also form a complete basis of orthonormal functions. There is a one-to-one correspondence between these two bases. It has to be noted that the eigenfunctions $\varphi_N(\vec{r}, t)$ coincide exactly with the eigenfunctions $u_n(\vec{r})$ when the instant value of the external field amplitude is equal to zero. Hence, these two bases coincide in the moments of time when $I(t) = 0$; what is more important, they coincide before and after the action of the laser pulse.

As mentioned above, the eigenfunctions $\varphi_N(\vec{r}, t)$ have the symmetry properties of the wave functions of the time-dependent Schrödinger Eq. (1). Therefore, it appears quite natural to use the basis of these functions in order to solve Eq. (1). However, due to the time derivative on the left-hand side of Eq. (1), the equations for the probability amplitudes of such expansion will inevitably include the integrals over the products of these eigenfunctions and their time derivatives. But the operator of boundary value problem (2) is time dependent; hence, the eigenfunctions of this problem and their time derivatives are not orthogonal. To overcome this problem the wave function $\psi(\vec{r}, t)$ can be initially expanded into a series of eigenfunctions $u_n(\vec{r})$,

$$\psi(\vec{r}, t) = \sum_{n,l} a_{n,l}(t) u_{n,l}(\vec{r}) + \int a(k, l, t) u(k, l, \vec{r}) dk,$$

and then the one-to-one correspondence of these two bases can be used. Whereas, moving from Eq. (1) to a set of equations for the probability amplitudes, the following integrals should be calculated:

$$\int u_n^* \left\{ \frac{1}{2m} \left[\vec{p} - \frac{e}{c} \vec{A}(t) \right]^2 + U(r) \right\} u_m dV.$$

It is convenient to use the following relations:

$$\begin{aligned} \int u_n^* \left\{ \frac{1}{2m} \left[\vec{p} - \frac{e}{c} \vec{A}(t) \right]^2 + U(r) \right\} u_m dV \\ = \sum_p V_{np}^{-1}(t) E_p V_{pm}(t), \end{aligned}$$

where we have used the relations between the base functions $u_n(\vec{r})$ and $\varphi_N(\vec{r}, t)$. Then, the set of differential equations for the population amplitudes of the discrete states and continuum quasistates becomes

$$i\hbar \frac{da_n}{dt} = \sum_{m,k} V_{nk}^{-1} E_k V_{km} a_m, \quad (3)$$

where E_k are the energy eigenvalues.

The spectrum of atomic response is determined by the equation for the atomic current density,

$$\vec{j}(\vec{r}, t) = \frac{q}{2m} \left[\psi^* \times \left(\vec{p} - \frac{q}{c} \vec{A} \right) \psi + \left[\left(\vec{p} - \frac{q}{c} \vec{A} \right) \psi \right]^* \times \psi \right]. \quad (4)$$

The spectrum of the atomic response in the far-field zone is given by [42,43]

$$\vec{A}_{\text{resp}}(\vec{r}, \omega) = \frac{\exp(ikr)}{rc} \int \vec{j}(\vec{r}', \omega) \exp(-i\vec{k}\vec{r}') dV'.$$

The field strength in the far-field zone is

$$\vec{E}_{\text{resp}}(\vec{r}, \omega) = -i \frac{\omega \exp(ikr)}{rc^2} [[\vec{J}(\omega) \times \vec{n}] \times \vec{n}],$$

where

$$\vec{J}(\omega) = \int \vec{j}(\vec{r}, \omega) dV,$$

and $[[\vec{J}(\omega) \times \vec{n}] \times \vec{n}]$ is a vector triple product.

As a result, the spectral and polarization properties of the generated photoemission spectrum follow those of the atomic current spectrum, which is [41] as follows:

$$\vec{J}(t) = i \sum_{n,m,p,q} a_n^*(t) a_m(t) \omega_{pq} V_{np}^{-1}(t) \vec{d}_{pq} V_{qm}(t), \quad (5)$$

where $a_n(t)$ are the probability amplitudes of the atomic states, \vec{d}_{pq} are matrix elements of the dipole momentum operator, and $\omega_{pq} = (E_p - E_q)/\hbar$. The relation between the matrix elements of the momentum operator and the dipole momentum operator from Ref. [41] is used in (5). It is seen from the last equations that the field strength is proportional to the time derivative of the atomic current.

It should be noticed that in all the equations above the atomic states are marked by the one-letter symbol (n). However, the atomic states of the three-dimensional (3D) boundary value problem depend on the three quantum numbers: the principal quantum number n , the orbital quantum number l , and its projection m . The one-letter symbols are used here for compactness only.

Equations (3) and (5) enable us to calculate the HHG spectrum at given parameters of the laser pulse interacting with an atom. The most important conclusion of the above discussion is that the atomic response on the action of the laser field with arbitrary polarization and amplitude temporal profiles can be simulated by using (3) and (5), i.e., the temporal profile of the laser field can be taken directly coinciding with those of real experiments. However, the set (3) includes an infinite number of equations. The infinite set of Eqs. (3) and (5) cannot be solved neither analytically nor numerically. On the other hand, at any finite amplitude of the laser field, only a certain

finite number of atomic states make an appreciable input in the atomic response. The main advantage of ‘‘an atom in the external field’’ basis is the following: the input of each state can be numerically calculated before the set of equations for probability amplitudes is solved. The accuracy of calculations with the help of any truncated basis at an arbitrary amplitude of the laser field can be exactly estimated. It should be also noted that each eigenfunction of ‘‘an atom in the external field’’ basis is the infinite series over the eigenfunction of the free-atom basis. So, in any truncated basis the whole basis of free-atom states is taken into account. The number and amplitudes of decomposition coefficients depend on the laser field amplitude.

In accordance with the selection procedure discussed above, in the case of the Ne atom and the laser pulse intensity of about $10^{14} \text{ W cm}^{-2}$, one should take into account the following limited number of ‘‘an atom in the external field’’ wave functions corresponding to the excited discrete states of the Ne energy spectrum: $2p$ (ground state), $3s$, $3p$, $3d$, $4s$, $4p$, $4d$, $4f$, $5s$, $5p$, $5d$, $5f$, and $6s$. It should be noticed that due to the wide spectral width of a femtosecond pulse it is assumed that the sublevels corresponding to different orbital momentum projections (m) for given l are populated equally.

On the basis of the theoretical model above, the Ne photoemission spectra have been calculated at different parameters of the laser pulses. The ellipticity and polarization angles of harmonics have been reconstructed with the help of the calculated Stokes parameters. To make a reliable comparison with the experimentally measured spectra, the transmission effects [44] and the material dispersion [45] have been taken into account for calculating the phase-matching effects for the harmonics with the help of Eq. (2) from Ref. [45] for ω and for 2ω [46]. The problem of the harmonic propagation in the atomic gas has been solved in the integral form where the solutions of the single atom problem are used as the field sources. The main influence of propagation effects is due to the dispersion which affects the frequency-angular spectra of emission.

In order to illustrate the good validity of the numerical model in standard conditions, the latter has been tested by simulating two standard cases which are quite clear for understanding. The first one is the study of the HHG generated by a noble gas in elliptically polarized laser light. An 800-nm elliptically polarized light of moderate intensity ($\sim 10^{14} \text{ W cm}^{-2}$, 38 fs) irradiating an Ar gas has been considered. For these simulations a very precise model of the Ar atom energy structure (it also contains excited states and their substates as the model described above) has been used. The results of the comparison between experimentally measured data, obtained on the same installation and close setup similar to Ref. [36] and corresponding simulations, are presented in Fig. 1. It shows good agreement for the considered H25 and H27 harmonics. Note that both these theoretical (filled squares for H25 and filled circles for H27) and experimental (open squares for H25 and open circles for H27) evolutions fit quite well the results presented recently in Ref. [47]. Moreover, the numerically calculated behavior demonstrates qualitative coincidence with the experimental results presented in Refs. [17,18] and obtained for pulses of longer duration. There is also a close coincidence with numerical calculations presented in Ref. [48].

In the second standard study, the case discussed in Ref. [40] has been represented: the two-color ($\omega + 2\omega$) orthogonally

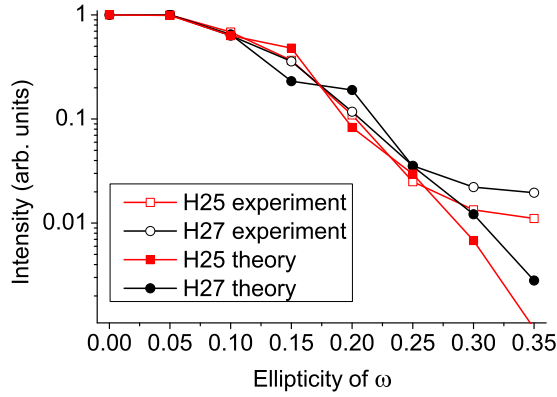


FIG. 1. Simulated H25 (filled squares), H27 (filled circles), measured H25 (open squares), and H27 (open circles) harmonics yields as a function of the laser field ellipticity in the single-color (800-nm laser wavelength) experiments.

polarized laser field interacting with the Ne atom has been simulated. This simulation implies low laser pulse intensities ($I_\omega \sim I_{2\omega} \sim 10^{13} \text{ W cm}^{-2}$) in order not to disturb strongly the ground state ($2p$), i.e., to avoid preexcitation and to boil down to the same assumptions which are in Ref. [40]. The intensities of ω and 2ω fields are then lower than those used in Ref. [40]. Yet, our objective was not in the here presented investigation to precisely describe their results but to show that, if the ground state is not preexcited, then the ellipticity of high harmonics cannot appear at these low intensities. Zero delay time between the pulses, zero value of the relative phase, and the same temporal width of 38 fs for the ω and 2ω pulses (FWHM) have been used as parameters of the calculation. The results are presented in Fig. 2. Figure 2(a) represents the temporal dependence of the ground state [the blue (upper) curve 1] and the sum of excited states [the pink (lower) curve 2] populations. It is clearly seen that, even in the region where the laser field achieves the maximum value, the population of the ground state is much higher than the one of all the excited states. Figure 2(b) shows that in these numerical conditions the generated spectrum contains linearly polarized odd and even harmonics. Most importantly, it also coincides with the interpretation described in Refs. [40,49], the odd and even harmonics being orthogonally polarized to each other and following the polarizations of ω and 2ω radiations, respectively.

To summarize, the two considered cases illustrate that our numerical model is able to reproduce some typical behavior of the HHG in standard conditions.

III. COMPARISON WITH EXPERIMENTAL DATA

In a second step, the consistency of our numerical model is demonstrated by simulating the experimental cases of Ref. [36]. With respect to the second standard study (see the previous section), it mainly differs by the likely preexcitation of the ground state, made possible at laser intensities of $\sim 10^{14} \text{ W cm}^{-2}$. In this scheme, the laser field radiation at the basic frequency of a Ti:Sa laser ($\lambda = 800 \text{ nm}$) is focused inside a 5-mm-long gas cell filled with 40 mbars of neon. After the lens, the BBO crystal is implemented directly inside the laser beam path, the position of the BBO crystal

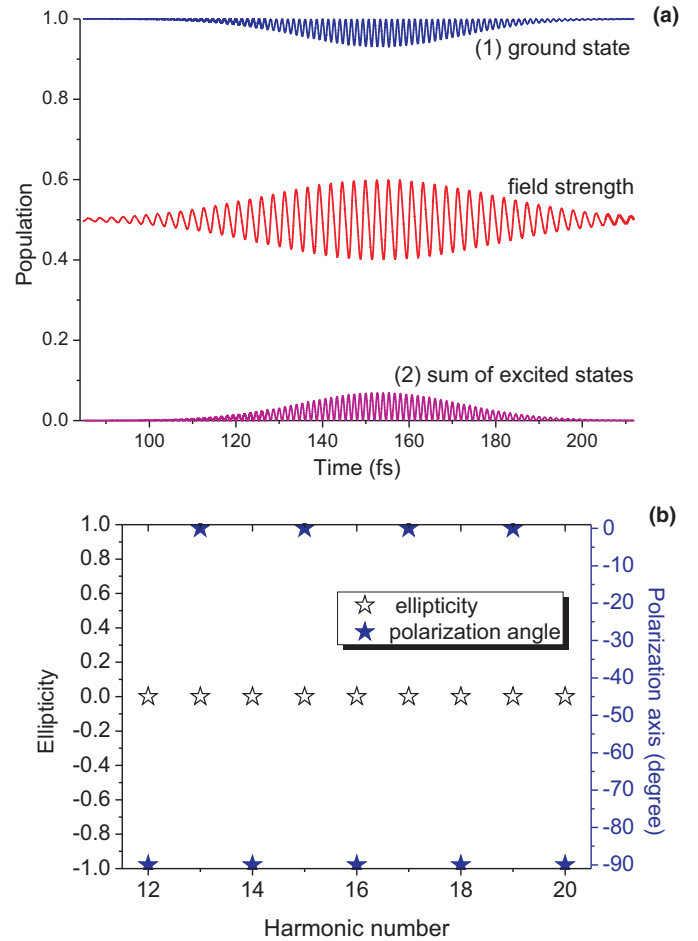


FIG. 2. (a) Calculated temporal behavior of the ground-state population [blue (upper) curve 1] and the sum of the excited-state populations [pink (lower) curve 2]. (b) Simulated ellipticity (open star) and polarization angle (blue star) as a function of harmonic orders. The case of a two-color orthogonally polarized laser field for which each corresponding laser pulse component has relatively low intensity (about $10^{13} \text{ W cm}^{-2}$) in order not to disturb strongly the ground state ($2p$) of the neon atoms.

axes corresponding to the perfect phase-matching conditions for the second-harmonic generation. After the crystal, the $\omega + 2\omega$ coherent field is present with components delayed by Δt having a phase shift of $\Delta\varphi = \pi/2$ and both with linear polarization but orthogonal to each other. The two-color field illuminates the Ne medium producing a burst of harmonics. In the experiments, BBO crystals of two different thicknesses have been used: 100 and 250 μm . The temporal delay between the ω and the 2ω pulses is equal to $\Delta t = 14$ and $\Delta t = 42$ fs, respectively. The variation of the crystal thickness results in the variation of the absolute and relative intensity of ω and 2ω fields: $I_\omega = 1.5 \times 10^{14}$, $I_{2\omega} = 1.3 \times 10^{13} \text{ W cm}^{-2}$ (for 100 μm), and $I_\omega = 3 \times 10^{14}$, $I_{2\omega} = 0.4 \times 10^{14} \text{ W cm}^{-2}$ (for 250 μm).

With these parameters, the temporal behavior of the ground and excited states becomes drastically different as compared to the previous case. The population of the ground state at the end of the pulses becomes much lower than those of the excited states (see Fig. 3 which is calculated for the case of 100 μm).

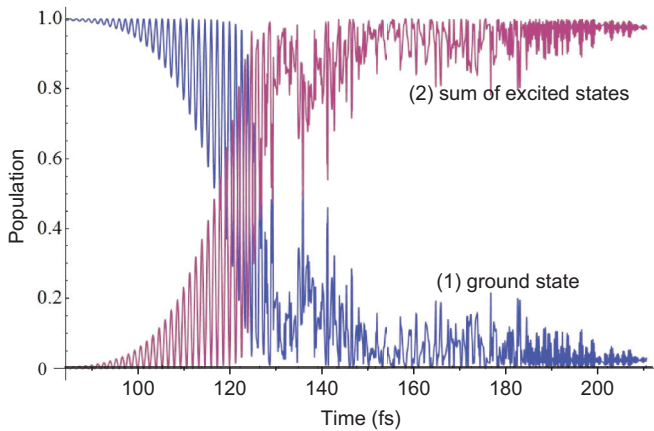


FIG. 3. Calculated temporal behavior of the ground-state population (blue curve 1) and the sum of the excited-state population (pink curve 2) for neon atoms. The case of Ref. [36] and a 100- μm -thick BBO crystal.

Comparisons between the theoretically calculated (stars) and the experimentally measured main characteristics of the harmonics are then presented in the coming section. For each characteristic, odd and even harmonics are presented separately for clarity. In Figs. 4(a) and 5(a), the ellipticity as a

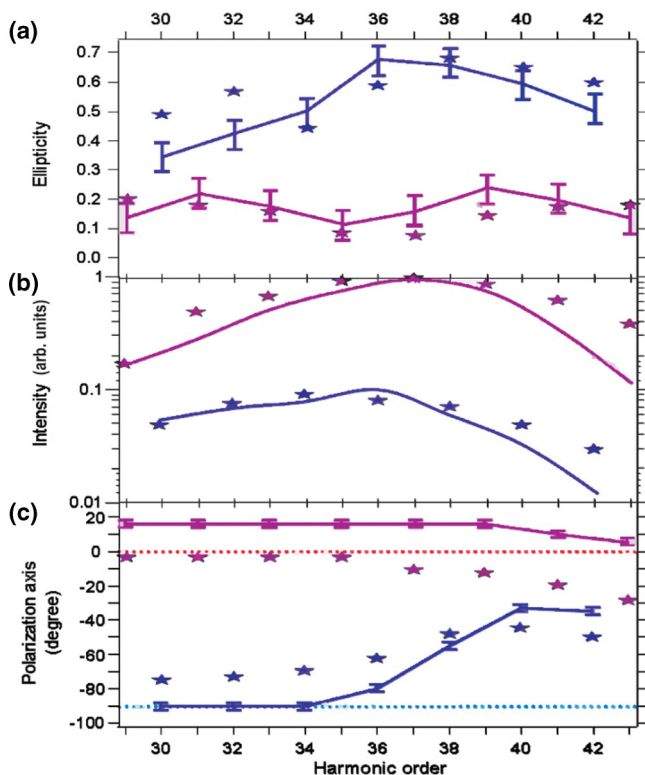


FIG. 4. (a) Measured (solid lines) and simulated (star) ellipticity, (b) intensity, and (c) polarization axis for the 100- μm -thick BBO crystal as functions of the harmonic orders: odd (pink) and even (violet). In (c) the dotted lines indicate the polarization axes of ω [red (upper)] and 2ω [blue (lower)]. Simulation points have been calculated for $I_\omega = 1.5 \times 10^{14}$, $I_{2\omega} = 1.3 \times 10^{13}$ W cm^{-2} , $\Delta t = 14$ fs, and $\Delta\varphi = \pi/2$.

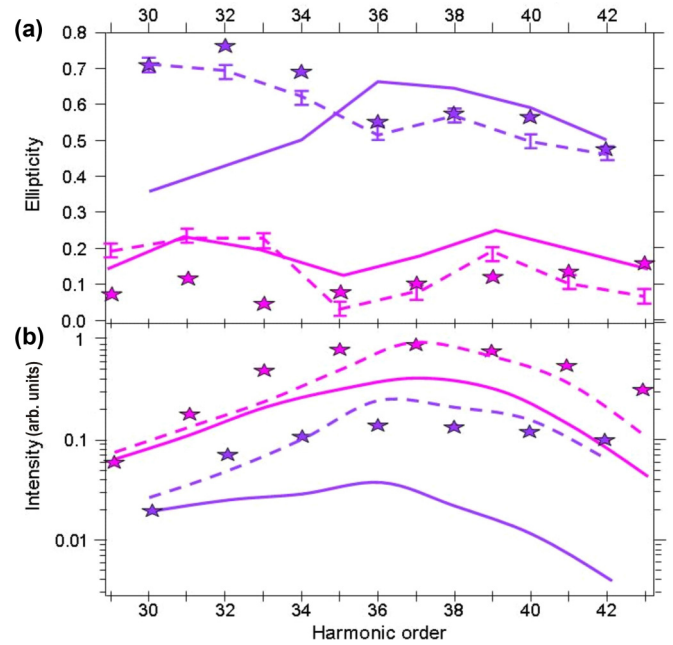


FIG. 5. (a) Measured (dashed lines) and simulated (stars) ellipticity and (b) intensity as functions of the harmonic order for odd (pink) and even (violet) harmonics for the case of a 250- μm -thick BBO crystal. Simulation points have been calculated for $I_\omega = 3 \times 10^{14}$ W cm^{-2} , $I_{2\omega} = 0.4 \times 10^{14}$ W/cm^{-2} , $\Delta t = 42$ fs, and $\Delta\varphi = \pi/2$. The 100- μm -thickness measured data (solid line, from Fig. 4) have been superimposed for direct comparison.

function of the harmonic order is shown for BBO crystal thickness equal to 100 and 250 μm , respectively, as used in Ref. [36]. The comparison in intensity is presented in Fig. 4(b) (100 μm) and Fig. 5(b) (250 μm). In order to calculate the harmonics intensities, the phase-matching conditions for both ω and 2ω waves [45] as well as the transmission of generated harmonics through the gas and filters (aluminum filter containing 2×10 nm of Al_2O_3) [44] have been taken into account. In Fig. 4(c) the direction of the polarization axis is shown as a function of the harmonic order. To summarize, Figs. 4 and 5 show evidently that the results of simulations reproduce accurately the results of measurements with both BBO thicknesses. Hence, the results of such a simulation can enable to provide a deep insight in the nature of the observed phenomena.

IV. DEGREE OF POLARIZATION

The results of the above simulations have been based on the single atom model. But in the *in situ* experiments, one has to deal with a gas cell, i.e., an extended atomic medium. Different atoms of the medium can emit radiations with different parameters. So, it is difficult to assume that the integral emission of the extended gas volume will be ideally polarized. To solve that, the polarization properties are studied for some specific harmonics. On the basis of the method presented in Ref. [48] both temporal and spatial degrees of polarization have been evaluated.

First, the part of the total atomic current density temporal distribution corresponding to the H36 and the H37 (these harmonics correspond to the maxima of spectra, see Fig. 5)

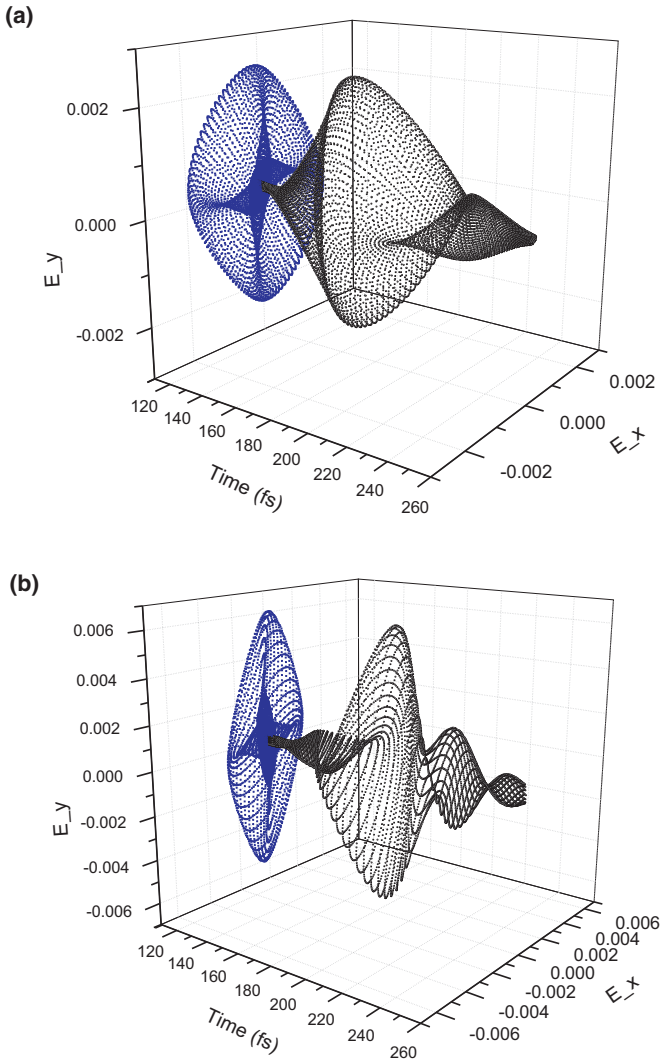


FIG. 6. Temporal behavior of the (a) H36 and (b) H37 harmonics calculated for the 100- μm -thick BBO crystal [black 3D curve] and its projections [blue (gray) curve] on the polarization axes of ω (corresponding to $E_x = 0$) and of 2ω ($E_y = 0$).

harmonics has been extracted by performing in sequence a Fourier transformation, the filtering by choosing a harmonic's peak, and its imaging over the Nyquist frequency and the inverse of the Fourier transformation. As a result, a temporal behavior of the field strength which is presented in Fig. 6(a) for H36 and in Fig. 6(b) for H37 has been obtained. The temporal behavior of the presented harmonics is quite homogeneous in time. To give some numerical characteristics of these dependencies, an integration over time has been made by using the formula (46), and then the degrees of ellipticity and polarization have been calculated by using formulas (44) and (45) from Ref. [48]. For H36/H37, respectively, 0.48/0.26 has been obtained for the degree of ellipticity, and 0.87/0.81 has been obtained for the degree of polarization. The ellipticity values are very close to the experimentally measured ones.

Second, the impact of the spatial properties of the gas media on the characteristics of the generated radiation has been studied on the basis of a model containing a chain of atoms placed on the focal plane of the laser beam. Accounting

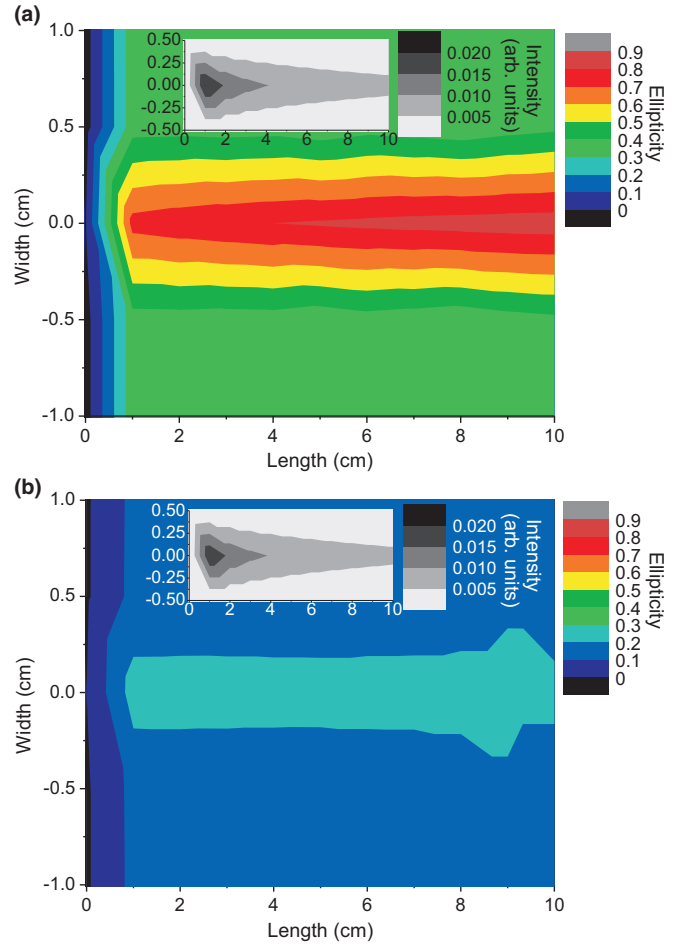


FIG. 7. Spatial mapping of ellipticity of the (a) H36 and (b) H37 harmonics generated by a chain of approximately 7×10^5 atoms calculated for the 100- μm -thick BBO crystal case. The inset: corresponding intensity spatial distributions of H36 and H37 harmonics.

for the Gaussian profile of the laser beam, the single atom photoemission spectrum has been calculated for the atoms placed in different transversal positions where the intensity of the laser beam is equal to 1, 0.9, 0.8, 0.5, and 0.3 of the maximal intensity. The single atom calculations provide us with the temporal behavior of the atomic current in vector form. In order to find the spatial distribution of some of the generated harmonics (H36, H37) the interpolations of the single atom data have been performed, and the response of the chain consisting of approximately 7×10^5 atoms has been calculated (in order to achieve a step between the atoms of less than 0.1 of the wavelength of the generated harmonic). The results [the ellipticity as well as the intensity (in the inset) distributions] are presented in Fig. 7, the laser pulse propagating from the left to the right. Due to the symmetry of the model (chain of atoms), the spatial intensity distributions have two peaks: One along the laser field propagation direction (Fig. 7), and one against it, symmetric to the previous one (not shown). Due to the small length of the chain (~ 1.5 mm) and divergence, the peak intensity of the generated radiation decreases along with the propagation distance, and at the same time, the width of the generated beam increases, so the energy remains constant.

The results presented in Fig. 7 are calculated with the help of formula (4) from Ref. [50]. To study the degree of polarization, a spatial integration in (46) has been made, and formulas (44) and (45) from Ref. [48] have been used. As a result, for H36/H37, respectively, 0.58/0.1 has been obtained for the degree of ellipticity, and 0.87/0.92 has been obtained for the degree of polarization. The obtained results demonstrate a high degree of polarization of the generated radiation.

V. ORIGIN OF ELLIPTICITY

In Sec. III good agreement between simulations and experimental measurements has been shown. Hence, the nonperturbative theory of light-atom interaction provides a reliable description of the observed phenomena. However, the account of a relatively large number of excited atomic states prevents an obvious interpretation. Here, the qualitative interpretation based on the use of a “one-level” approximation is provided in the case of high driving intensities.

The atomic current is given by

$$\vec{J}(t) = \sum_{\substack{n_1 l_1 m_1 \\ n_2 l_2 m_2}} a_{n_1 l_1 m_1}^*(t) a_{n_2 l_2 m_2}(t) \langle n_1 l_1 m_1 | \vec{j} | n_2 l_2 m_2 \rangle,$$

where the summation includes all the atomic states characterized by the principal quantum number n , the angular momentum l , and its projection m . The matrix elements of atomic current density are as follows:

$$\begin{aligned} \langle n_1 l_1 m_1 | \vec{j} | n_2 l_2 m_2 \rangle \\ = i \sum_{n_3 l_3 m_3 n_4 l_4 m_4} \omega_{n_3 l_3 m_3 n_4 l_4 m_4} \langle n_1 l_1 m_1 | V^{-1}(t) | n_3 l_3 m_3 \rangle \\ \times \langle n_3 l_3 m_3 | \vec{d} | n_4 l_4 m_4 \rangle \langle n_4 l_4 m_4 | V(t) | n_2 l_2 m_2 \rangle. \end{aligned} \quad (6)$$

On the basis of the hydrogenlike wave functions the matrix elements of operator V are calculated analytically and have the form of

$$\begin{aligned} \langle n_2 l_2 m_2 | V^{-1} | n_1 l_1 m_1 \rangle = \sum_{l=|l_1-l_2|}^{l_1+l_2} \sum_{m=-l}^l Y_{lm}^*(\vec{e}(t)) C(lm | l_2 m_2, l_1 m_1) \\ \times \langle n_2 l_2 | j_l \left(\frac{q}{\hbar c} A(t)r \right) | n_1 l_1 \rangle, \end{aligned} \quad (7)$$

where

$$\begin{aligned} C(lm | l_2 m_2, l_1 m_1) \\ = i^{l_1-l_2} (-1)^{m_1} \begin{pmatrix} l_2 & l & l_1 \\ m_2 & m & -m_1 \end{pmatrix} \begin{pmatrix} l_2 & l & l_1 \\ 0 & 0 & 0 \end{pmatrix} \\ \times \sqrt{4\pi(2l+1)(2l_1+1)(2l_2+1)}, \\ \langle n_2 l_2 | j_l \left(\frac{q}{\hbar c} A(t)r \right) | n_1 l_1 \rangle \\ = \int_0^\infty R_{n_2 l_2}(r) j_l \left(\frac{q}{\hbar c} A(t)r \right) R_{n_1 l_1}(r) r^2 dr. \end{aligned}$$

According to Eq. (6), the direction of the atomic current orientation depends on the orientation of the atomic dipole momentum, which is the quantum-mechanical average of the atomic electron radius vector. On the other hand, the matrix

elements $V_{nm}(t)$ depend on the mutual orientation of the laser pulse field and the angular momentum of atomic electron. Hence, the atomic current depends in tensor form on the laser field, polarization vector, and the atomic angular momentum, the orientation of which determines the orientation of matrix elements \vec{d}_{nm} [41].

At subatomic laser field strength, the ground state ($|0\rangle$) is basically populated, and it results in $\vec{J}(t) = \langle 0 | \vec{j}(\vec{r}, t) | 0 \rangle$, where

$$\begin{aligned} \langle 0 | \vec{j} | 0 \rangle = i \sum_{n_1 l_1 m_1} \sum_{n_2 l_2 m_2} \omega_{n_1 l_1 m_1 n_2 l_2 m_2} \langle 0 | V^{-1} | n_1 l_1 m_1 \rangle \\ \times \langle n_1 l_1 m_1 | \vec{d} | n_2 l_2 m_2 \rangle \langle n_2 l_2 m_2 | V | 0 \rangle. \end{aligned} \quad (8)$$

Neon gas was used in the experiments. The ground state of Ne is a $2p$ state $|0\rangle = |n=2, l=1\rangle$, which actually has three sublevels corresponding to different values of m ($m=0, \pm 1$). The dependence of matrix elements $\langle n_1 l_1 | j_l | n_2 l_2 \rangle$ on the quantum numbers $n_{1,2}$ and $l_{1,2}$ was investigated in Ref. [51]. In the subatomic region of the laser field strength this dependence is $\langle n_1 l_1 | j_l | n_2 l_2 \rangle \propto \mu_0^{|l_2-l_1|}$, where $\mu_0 = qA_0 a_B / \hbar c$. The selection rules for dipole matrix elements have the form of $l_2 - l_1 = \pm 1$. As a result, even in the subatomic region of laser field strength where the ground state is basically populated, the atomic current (8) due to summations over (n_1, l_1, m_1) and (n_2, l_2, m_2) includes the inputs of all other atomic states. The use of the term one level is due only to the assumption that $a_{nlm}(t) \approx \delta_{n|0} \delta_{l|0}$. That is why the simplified model, called one-level approximation, includes really the three sublevels of the $2p$ state corresponding to different m 's as well as selected previously excited states and the sublevels corresponding to them. For simplicity only $3s(1)$ and $3d(2)$ states are shown in the equations below, whereas the additional states do not change the angular dependences (this is true only for one-level approximation described above).

Thus, the matrix elements of the atomic current in the one-level approximation have the form of

$$\langle 0 | \vec{j} | 0 \rangle = \sum_{m_1 m_2} \langle 2, 1, m_1 | \vec{j} | 2, 1, m_2 \rangle. \quad (9)$$

Simplifying the designation of matrix elements by writing $\langle 2, 1, m_1 | \vec{j} | 2, 1, m_2 \rangle = \langle m_1 | \vec{j} | m_2 \rangle$, one can represent the set of matrix elements in a form of the following matrix:

$$\begin{pmatrix} \langle 1 | \vec{j} | 1 \rangle & \langle 1 | \vec{j} | 0 \rangle & \langle 1 | \vec{j} | -1 \rangle \\ \langle 0 | \vec{j} | 1 \rangle & \langle 0 | \vec{j} | 0 \rangle & \langle 0 | \vec{j} | -1 \rangle \\ \langle -1 | \vec{j} | 1 \rangle & \langle -1 | \vec{j} | 0 \rangle & \langle -1 | \vec{j} | -1 \rangle \end{pmatrix}. \quad (10)$$

The elements of the matrix (10) obey the following properties. First of all, the sum of the diagonal elements of the matrix (10) is

$$\begin{aligned} \sum_{m=-1}^{+1} \langle m | \vec{j} | m \rangle = -\frac{2}{5} \{ 5\omega_1 d_{10} \langle 1 | j_1(z) | 0 \rangle \langle 1 | j_0(z) | 1 \rangle \\ - 2 \langle 1 | j_2(z) | 1 \rangle + 2\omega_2 d_{12} [5 \langle 1 | j_0(z) | 1 \rangle \\ \times \langle 1 | j_1(z) | 2 \rangle - \langle 1 | j_2(z) | 1 \rangle \langle 1 | j_1(z) | 2 \rangle \\ - 9 \langle 1 | j_3(z) | 2 \rangle] \} [\vec{e}_x \cos \varphi + \vec{e}_y \sin \varphi \\ \times \sin \theta + \vec{e}_z \cos \theta], \end{aligned} \quad (11)$$

where \vec{e}_α are the unit vectors of axes in the atomic configuration space, i.e., in the Cartesian coordinate set with the z axis coinciding with the direction of atom angular momentum $\langle \vec{l} \rangle$. Angles θ and φ determine the orientation of the laser field polarization vector,

$$\vec{e}(t) = \frac{\vec{A}(t)}{A(t)} = (\vec{e}_x \cos \varphi + \vec{e}_y \sin \varphi) \sin \theta + \vec{e}_z \cos \theta.$$

Equation (11) clearly demonstrates that the atomic current and the harmonic polarization vectors at each moment of time follow the laser field polarization vector.

Thus, the polarization properties of the atomic current (9) associated with the diagonal elements of the matrix (10) coincide with the polarization properties of the incident laser field. For example, if the incident laser field consists of two-color orthogonally polarized $\omega + 2\omega$ components, then, the polarization of odd and even harmonics will be mutually orthogonal. The polarization vector of odd (respectively, even) harmonics will follow the polarization vector of fundamental (respectively, second-harmonic) radiation. This is due to the fact that the matrix elements of the dipole moment operator have a nonzero value only for transitions between the states of opposite parity. Hence, the matrix elements of operator V in Eq. (8) ($\langle 0|V^{-1}|1\rangle$ and $\langle 2|V|0\rangle$) are the functions of opposite parity with respect to $A(t)$ (see Ref. [41]). As a result, the right-hand side of (8) is the product of $\vec{A}(t)$ and the even function of $A(t)$. When

$$\vec{A}(t) = \vec{e}_1 A_1(t) \cos \omega t + \vec{e}_2 A_2(t) \cos 2\omega t,$$

and \vec{e}_1 and \vec{e}_2 are orthogonally polarized, the odd and even harmonics become as well orthogonally polarized to each other.

The above conclusion coincides with the one for the s ground state (which can be easily shown) and with the one obtained in Ref. [40].

Second, the sum of the matrix elements of the matrix (10) with $\Delta m = \pm 1$ results in

$$\langle 1|\vec{j}|0\rangle + \langle 0|\vec{j}|-1\rangle + \langle 0|\vec{j}|1\rangle + \langle -1|\vec{j}|0\rangle = 0. \quad (12)$$

It should be noted that, despite the fact that each term of the sum in (12) is not equal to zero and that it has a polarization dependence which differs from the one presented in (11), their sum is equal to zero. This zero value is due to the symmetry reasons, and any breaking of the symmetry by, for example, implementing additional external fields will lead to a nonzero impact of the matrix elements with $\Delta m = \pm 1$ and, as a consequence, to the direction of the atomic current not coinciding with the laser field polarization.

The residual components of the matrix (10) are the atomic current matrix elements corresponding to $\Delta m = \pm 2$. These matrix elements have the symmetry properties which are drastically different from those of the incident laser field. Even in the case of the Ne atom the equations for these components are very overcomplicated; therefore, only the functional dependency of the projection of the sum of these matrix elements to the x axis in atomic configuration space is

shown

$$\begin{aligned} \vec{e}_x \left(\langle n_0 l_0 m_0 = +1 | \vec{j} | n_0 l_0 m_0 = -1 \rangle \right. \\ \left. + \langle n_0 l_0 m_0 = -1 | \vec{j} | n_0 l_0 m_0 = +1 \rangle \right. \\ \left. - \sum_{m=-1}^{+1} \langle n_0 l_0 m | \vec{j} | n_0 l_0 m \rangle \right) \\ = \sin \theta \{ [f_1(t) + f_2(t) \cos(2\theta)] \cos \varphi + f_3(t) \cos(3\varphi) \sin^2 \theta \}. \end{aligned} \quad (13)$$

Equation (13) includes trigonometrical functions of angles θ and φ and their products. This leads to a dramatic change in the polarization state of the generated harmonics in comparison with the laser field.

Note that the impact of different sublevels of the p ground state was also studied in Ref. [49]. Using a simpler model (only one bound state was taken into consideration) the influence of the sublevels on the harmonic spectrum and polarization was studied especially in the near cutoff region.

Thus, the analytical approach based on the one-level approximation provides a deep insight into the physics of high harmonic ellipticity origin. In the frame of the light-atom interaction theory based on a dipole approximation, the atomic response is prescribed by the selection rules for the dipole transitions. At the same time, in the frame of the nonperturbative theory, the atomic response is determined by the matrix elements of operator V [see Eq. (7)]. Operator V includes all powers of operator \vec{r} . So, the initial and the final states of the cascade transitions do not obey certain selection rules. The analysis given above shows that the ellipticity of harmonics is mainly due to the matrix elements of atomic current which are most unusual for the dipole approximation approach. For example, in the case of the $2p$ state of the Ne atom, these matrix elements bind the sublevels of $m = +1$ and $m = -1$. This conclusion is an exact analytical result obtained in the frame of the one-level approximation. At the same time, the results of numerical simulations presented in the previous section show evidently that, if this approximation is freed up, one will have harmonics of high ellipticity, and it is a strong belief that the origin of this phenomena is exactly the same. In other words, the following transitions between all the sublevels of the Ne states (with $|\Delta m| \geq 2$, especially for d and f excited states) are accounted for in high ellipticity HHG processes, even if the intensities of ω and 2ω are decreased. The given discussion provides the hint that the polarization properties of the response field associated with the atomic current matrix elements of the maximal Δm are mostly different from that for the incident field. When we take into account the excited atomic states the number of such terms increases. The numerically calculated atomic current (5) includes, for example, the following term:

$$\begin{aligned} \langle 3, 2, -2 | V^{-1} | 2, 1, -1 \rangle (\omega_{2,1,-1} - \omega_{3,0,0}) \\ \times \langle 2, 1, -1 | \vec{d} | 3, 0, 0 \rangle \langle 3, 0, 0 | V | 4, 1, 1 \rangle. \end{aligned}$$

On one hand, all matrix elements here are the matrix elements for the dipole allowed transitions. But, on the other hand, the resultant matrix element is the matrix element

with $|\Delta m| = |-2 - 1| = 3$, i.e., $|\Delta m| \geq 2$. That is why for describing experimentally observed phenomenon excited states have to be included. However, it does not mean that other transitions (and even dipole forbidden) are not allowed. All transitions between all states and substates are accounted with their own weight, which depends nonlinearly on the laser field strength.

Note that it is possible, however, to have ellipticities in the case of $|\Delta m| = 1$, especially experimentally, when beams are focused inside a gas medium since their corresponding waves are not planes anymore. For calculations in which plane waves are assumed, highly elliptical harmonics can be produced when excited states are populated (in order to include transitions with $|\Delta m| = 2$).

VI. CONCLUSIONS

The nonperturbative theory of the light-atom interaction was applied to model numerically the results of experimental measurements for a configuration in which two-color laser beams having orthogonal linear polarizations interact with a noble gas and generate high-order harmonics with high ellipticity. The single atom model taking into account the excited states was first validated on the standard effects of the HHG, i.e., from a single-color laser field with elliptical polarization and from a two-color laser field with orthogonal polarization in the low intensity regime. Second, the model was used to simulate the experimentally measured properties

of the generated high harmonics, such as intensity, ellipticity, and the polarization axis [36]. Comparison between simulations and experimental results showed good agreement. In addition, the degree of polarization was evaluated and was demonstrated to be high. Finally, the origin of the high value of harmonics ellipticity was studied analytically, leading to the conclusion that this phenomenon comes from the fact that sublevels are populated with different projections of the orbital quantum numbers of the atomic states. Mathematically, this phenomenon comes from the fact that in the frames of nonperturbative theory the atomic current depends in tensor form on the laser field polarization vector and the atomic angular momentum. This tensor includes the terms which do not appear in the frame of perturbation theory approaches. The contribution of these terms to the amplitude of the response field increases along with the increase in driving laser field intensity.

ACKNOWLEDGMENTS

S.S. and A.A. thank the Russian Foundation for Basic Research (RFBR Grants No. 15-02-04352 and No. 16-32-00723). The work was supported by the ERC X-five (Contract No. 339128) and by the French Agence Nationale de la Recherche (ANR) under Grant No. NT09491966 (FEMTO-X-MAG) “Nanoscale imaging of femtosecond magnetization dynamics by the scattering of coherent soft x-ray laser harmonics.” G.L. and S.S. thank V. Malka and A. Lifschitz for support and fruitful discussions.

-
- [1] T. Popmintchev *et al.*, *Science* **336**, 1287 (2012).
 - [2] P. B. Corkum, *Phys. Rev. Lett.* **71**, 1994 (1993).
 - [3] J. Itatani *et al.*, *Nature (London)* **432**, 867 (2004).
 - [4] R. A. Ganeev, *Phys.-Usp.* **56**, 772 (2013).
 - [5] F. M. Lu, Y. Q. Xia, S. Zhang, and D. Y. Chen, *Laser Phys.* **23**, 115302 (2013).
 - [6] E. J. Takahashi, T. Kanai, K. L. Ishikawa, Y. Nabekawa, and K. Midorikawa, *Phys. Rev. Lett.* **99**, 053904 (2007).
 - [7] J. B. Bertrand, H. J. Wörner, H.-C. Bandulet, É. Bisson, M. Spanner, J.-C. Kieffer, D. M. Villeneuve, and P. B. Corkum, *Phys. Rev. Lett.* **106**, 023001 (2011).
 - [8] P. M. Paul *et al.*, *Science* **292**, 1689 (2001).
 - [9] A. Ozawa *et al.*, *Opt. Express* **16**, 6233 (2008).
 - [10] A. L’Huillier and P. Balcou, *Phys. Rev. Lett.* **70**, 774 (1993).
 - [11] S. Watanabe, K. Kondo, Y. Nabekawa, A. Sagisaka, and Y. Kobayashi, *Phys. Rev. Lett.* **73**, 2692 (1994).
 - [12] C. Jin, G. Wang, H. Wei, A.-T. Le, and C. D. Lin, *Nat. Commun.* **5**, 4003 (2014).
 - [13] L. E. Chipperfield, J. S. Robinson, J. W. G. Tisch, and J. P. Marangos, *Phys. Rev. Lett.* **102**, 063003 (2009).
 - [14] F. A. Weihe and P. H. Bucksbaum, *J. Opt. Soc. Am. B* **13**, 157 (1996).
 - [15] P. Antoine, B. Carré, A. L’Huillier, and M. Lewenstein, *Phys. Rev. A* **55**, 1314 (1997).
 - [16] V. V. Strelkov, A. A. Gonoskov, I. A. Gonoskov, and M. Y. Ryabikin, *Phys. Rev. Lett.* **107**, 043902 (2011).
 - [17] K. S. Budil, P. Salières, A. L’Huillier, T. Ditmire, and M. D. Perry, *Phys. Rev. A* **48**, R3437(R) (1993).
 - [18] P. Dietrich, N. H. Burnett, M. Ivanov, and P. B. Corkum, *Phys. Rev. A* **50**, R3585 (1994).
 - [19] H. Eichmann, A. Egbert, S. Nolte, C. Momma, B. Wellegehausen, W. Becker, S. Long, and J. K. McIver, *Phys. Rev. A* **51**, R3414(R) (1995).
 - [20] X.-M. Tong and S.-I. Chu, *Phys. Rev. A* **58**, R2656(R) (1998).
 - [21] B. Borca, A. V. Flegel, M. V. Frolov, N. L. Manakov, D. B. Milošević, and A. F. Starace, *Phys. Rev. Lett.* **85**, 732 (2000).
 - [22] D. B. Milosevic, W. Becker, and R. Kopold, *Phys. Rev. A* **61**, 063403 (2000).
 - [23] X. Xie, A. Scrinzi, M. Wickenhauser, A. Baltuška, I. Barth, and M. Kitzler, *Phys. Rev. Lett.* **101**, 033901 (2008).
 - [24] A. Husakou, F. Kelkensberg, J. Herrman, and M. J. J. Vrakking, *Opt. Express* **19**, 25346 (2011).
 - [25] L. Z. Liu, K. O’Keeffe, and S. M. Hooker, *Opt. Lett.* **37**, 2415 (2012).
 - [26] K. J. Yuan and A. D. Bandrauk, *Phys. Rev. Lett.* **110**, 023003 (2013).
 - [27] A. Fleischer, P. Sidorenko, and O. Cohen, *Opt. Lett.* **38**, 223 (2013).
 - [28] A.-T. Le and C. D. Lin, *J. Mod. Opt.* **58**, 1158 (2011).
 - [29] K.-J. Yuan and A. D. Bandrauk, *Phys. Rev. A* **84**, 023410 (2011).
 - [30] O. E. Alon, V. Averbukh, and N. Moiseyev, *Phys. Rev. Lett.* **80**, 3743 (1998).
 - [31] X. Zhou, R. Lock, N. Wagner, W. Li, H. C. Kapteyn, and M. M. Murnane, *Phys. Rev. Lett.* **102**, 073902 (2009).
 - [32] M. Kitzler and M. Lezius, *Phys. Rev. Lett.* **95**, 253001 (2005).
 - [33] B. Vodungbo *et al.*, *Opt. Express* **19**, 4346 (2011).

- [34] A. Fleischer, O. Kfir, T. Diskin, P. Sidorenko, and O. Cohen, *Nat. Photon.* **8**, 543 (2014).
- [35] A. Ferré *et al.*, *Nat. Photon.* **9**, 93 (2015).
- [36] G. Lambert *et al.*, *Nat. Commun.* **6**, 6167 (2015).
- [37] S. Long, W. Becker, and J. K. McIver, *Phys. Rev. A* **52**, 2262 (1995).
- [38] M. Ivanov and E. Pisanty, *Nat. Photon.* **8**, 501 (2014).
- [39] E. Pisanty, S. Sukiasyan, and M. Ivanov, *Phys. Rev. A* **90**, 043829 (2014).
- [40] D. Shafir *et al.*, *New J. Phys.* **12**, 073032 (2010).
- [41] A.V. Andreev, S. Y. Stremoukhov, and O. A. Shoutova, *Eur. Phys. J. D* **66**, 16 (2012).
- [42] L. D. Landau and E. M. Lifshitz, in *The Classical Theory of Fields*, 4th ed. (Butterworth-Heinemann, Oxford, 1980), p. 186.
- [43] J. D. Jackson, in *Classical Electrodynamics*, 3rd ed. (Wiley, New York, 1999).
- [44] http://henke.lbl.gov/optical_constants/
- [45] T. Popmintchev *et al.*, *Proc. Natl. Acad. Sci. USA* **106**, 10516 (2009).
- [46] K. B. Dinh, H. V. Le, P. Hannaford, and L. V. Dao, *J. Appl. Phys.* **115**, 203103 (2014).
- [47] S. D. Khan *et al.*, *CLEO: 2011—Laser Applications to Photonic Applications*, OSA Technical Digest (CD) (Optical Society of America, Washington, DC, 2011), Paper JWA88.
- [48] P. Antoine, A. L’Huillier, M. Lewenstein, P. Salières, and B. Carré, *Phys. Rev. A* **53**, 1725 (1996).
- [49] T. S. Sarantseva, M. V. Frolov, N. L. Manakov, M. Y. Ivanov, and A. F. Starace, *J. Phys. B: At., Mol. Opt. Phys.* **46**, 231001 (2013).
- [50] S. Y. Stremoukhov and A. V. Andreev, *Laser Phys. Lett.* **12**, 015402 (2015).
- [51] A. V. Andreev, R. A. Ganeev, H. Kuroda, S. Y. Stremoukhov, and O. A. Shoutova, *Eur. Phys. J. D* **67**, 22 (2013).